Theoretical and Applied Mechanics Letters 12 (2022) 100315

Contents lists available at ScienceDirect

Theoretical and Applied Mechanics Letters

journal homepage: www.elsevier.com/locate/taml

Letter

A universal bifurcation mechanism arising from progressive hydroelastic waves

Zhan Wang [a,b,*]

[a] Institute of Mechanics, Chinese Academy of Sciences, Beijing 100190, China
[b] School of Engineering Science, University of Chinese Academy of Sciences, Beijing 100049, China

ARTICLE INFO

Article history:
Received 5 December 2021
Accepted 12 December 2021
Available online 18 December 2021

Keywords:
Nonlinear wave
Supercritical bifurcation
Hydroelastic wave
Wavepacket

ABSTRACT

A unidirectional, weakly dispersive nonlinear model is proposed to describe the supercritical bifurcation arising from hydroelastic waves in deep water. This model equation, including quadratic, cubic, and quartic nonlinearities, is an extension of the famous Whitham equation. The coefficients of the nonlinear terms are chosen to match with the key properties of the full Euler equations, precisely, the associated cubic nonlinear Schrödinger equation and the amplitude of the solitary wave at the bifurcation point. It is shown that the supercritical bifurcation, rich with Stokes, solitary, generalized solitary, and dark solitary waves in the vicinity of the phase speed minimum, is a universal bifurcation mechanism. The newly developed model can capture the essential features near the bifurcation point and easily be generalized to other nonlinear wave problems in hydrodynamics.

It is well known that there exist two types of solitary waves in water waves, namely gravity solitary waves in shallow water and gravity-capillary solitary waves in deep water, and their bifurcation mechanisms are very different. Gravity solitary waves in shallow water, which exist above the phase speed maximum, decay monotonically in the direction of wave propagation and can be approximated by the sech-squared solitons of the celebrated Korteweg-de Vries (KdV) equation. However, gravity-capillary solitary waves in deep water, which exist below the phase speed minimum, feature oscillatory decaying tails and bifurcate from infinitesimal periodic waves [3,4]. Akylas [3] elucidated that the envelopes of gravity-capillary solitary waves can be well described by the nonlinear Schrödinger (NLS) equation with cubic nonlinearity. Therefore, these waves are usually called wavepacket solitary waves in the literature. Akylas also gave the condition for wavepacket solitary waves: a phase speed extremum achieved at a non-zero wavenumber and a focusing cubic NLS equation at this point.

However, Laget and Dias in 1997 computed interfacial capillary-gravity solitary waves between two semi-infinite fluids. They showed that when the density ratio of the upper to lower fluids is greater than 0.283, wavepacket solitary waves still exist; however, the branch does not bifurcate from infinitesimal periodic waves [8]. Dias and his collaborators [1,6] conducted the normal form analysis. They found that the cubic NLS equation is of defocusing type at the minimum of the phase speed in this situation. Therefore, a further asymptotic expansion needs to be carried out, such that the cubic-quintic NLS equation can explain the existence of these unusual solutions. This fact indicates that the focusing NLS equation is not necessary for wavepacket solitary waves.

Based on the Kirchhoff-Love plate theory, Părău and Dias in 2002 investigated hydroelastic solitary waves, which deal with the interaction between moving loads and deformable sheets that have wide usage in marine structures and sea transport [13,14]. Their analysis showed that there exists a critical depth H_c where the associated cubic NLS at the phase speed minimum changes the type. Milewski et al. in 2011 revisited the problem and found that even though small-amplitude solitary waves are not predicted to exist in deep water by standard perturbation analyses due to the defocusing nature of the NLS equation, solitary waves with finite amplitude do exist in the full Euler equations, a phenomenon similar to interfacial capillary-gravity waves. Taking advantage of the novel numerical scheme, Milewski et al. [12] continued the branch to explore the bifurcation mechanism of these large-amplitude solitary waves. It is shown in Fig. 1 that they occur along a branch of generalized solitary waves that itself bifurcates from periodic waves of

* Corresponding author.
E-mail address: zwang@imech.ac.cn

https://doi.org/10.1016/j.taml.2021.100315

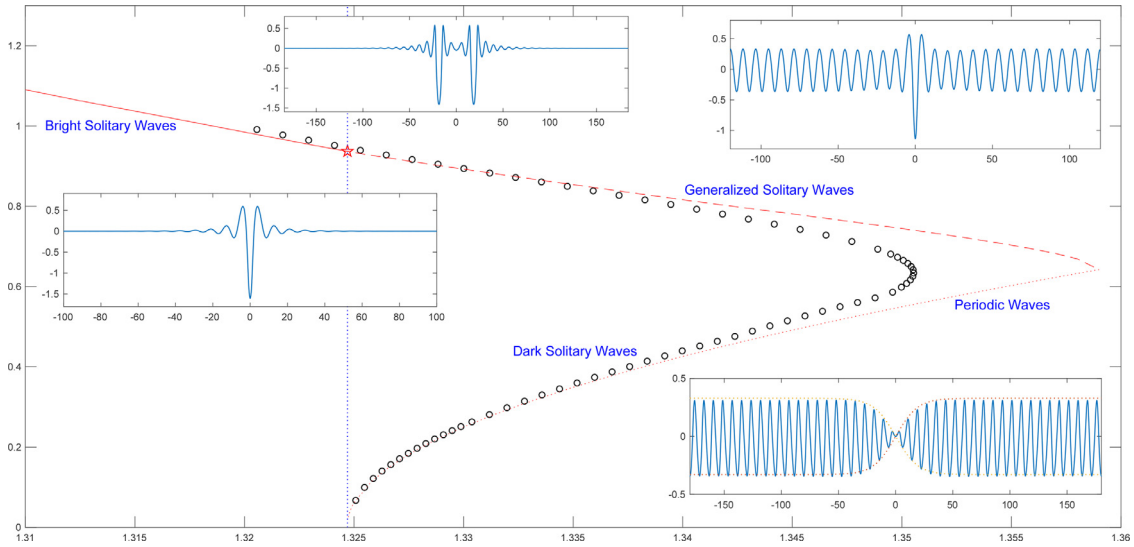

Fig. 1. Speed-amplitude bifurcation diagram of hydroelastic waves near the phase speed minimum $c_{\min} = 1.3247$ (vertical dotted line). The solutions are computed in the full Euler equations with the Kirchhoff-Love plate model. The amplitude is defined as $(\max\eta - \min\eta)/2$, where η is the wave profile. The uppermost curve is a branch of bright solitary waves for $c < c_{\min}$ (solid red line) and generalized solitary waves for $c > c_{\min}$ (dashed red line) which are distinguished from one another at the point (1.3247,0.9370) (labeled with a pentagram). The branches originating at $c_{\min}$ are periodic Stokes solutions (dotted red line) and dark solitary waves (black circles). Typical profiles for bright solitary wave (left), generalized solitary wave (upper right), dark solitary wave (lower right), and multi-packet bright solitary wave (upper middle) are plotted.

finite amplitude. We call this new bifurcation mechanics the 'supercritical bifurcation' since the branch first grows in the supercritical regime until a turning point that leads it to the subcritical regime. On the other hand, Milewski et al. in 2013 computed dark solitary waves predicted by the defocusing NLS equation whose envelope approaches a non-zero constant state in the far field and decreases to zero at the origin (see the embedded image in the bottom right corner of Fig. 1). The branch of dark solitary waves in hydroelastic waves stems from the bifurcation point with zero amplitude and also features a turning point. If one traces the upper branch by decreasing wave speed, traveling-wave solutions become multi-packet bright solitary waves once the wave speed reaches the subcritical regime. In summary, the bifurcation of deep-water hydroelastic waves near the critical speed, rich with Stokes, solitary, generalized solitary, and dark solitary waves, is of a novel type. This type of bifurcation was also found later in other hydrodynamic problems, including interfacial capillary-gravity waves [16], electrohydrodynamic surface waves under a vertical electric field [9], and hydroelastic waves with constant vorticity [7], indicating its universal property. Though this new bifurcation mechanism was numerically found in the full Euler equations under various situations, it is still necessary to propose a simplified model like the KdV equation to gravity waves in shallow water and the cubic NLS equation to gravity-capillary waves in deep water.

To study the stability and dynamics of capillary-gravity waves in deep water, Akers and Milewski (2009) [17] proposed a reduced model that generalized the famous Whitham equation (see Ref. for example). They expanded the linear dispersion relation near the phase speed minimum and fixed the coefficient of the quadratic nonlinearity by matching the coefficient of the cubic nonlinearity in the associated NLS equation. This model was further generalized to include forcing and viscosity to validate the laboratory experiments on symmetric and asymmetric shedding of capillary-gravity lumps [5,10]. Motivated by the work of Akers and Milewski [2], we in this paper extend their idea via introducing cubic and quartic nonlinear terms to acquire more degrees of freedom, and hence achieve the defocusing NLS equation and mimic the new bifurcation. The newly proposed model is simple enough and can capture the main features of the bifurcation mechanism. The rest of the paper is structured as follows. The detailed derivations of the model equation and the associated NLS equation are described. Then, the numerical results for both two- and three-dimensional problems are presented and discussed.

We take the problem of hydroelastic waves as an example to demonstrate the procedure of modeling. Following Refs. [11,12,15], we consider two-dimensional (2D) hydroelastic waves in deep water based on the nonlinear Kirchhoff-Love plate theory. First of all, the linear dispersion relation of the problem reads $\omega^2 = |k|\left(1+k^4\right)$ with ω the wave frequency and k the wavenumber, which has a phase minimum $c_{\min} = 2\times 3^{-\frac{3}{8}} \approx 1.3247$ at $k^* = 3^{-\frac{1}{4}} \approx 0.7598$. Since we are interested in the bifurcation mechanism of progressive waves of permanent form in the vicinity of this particular point, a narrow band approximation and unidirectional propagation of waves are assumed. Following Ref. [2], we expand the dispersion relation about $|k| = k^*$ as a Taylor series and retain terms up to quadratic order:

$$\omega(k) \approx \mathrm{sgn}(k)\left[\Omega(k^*) + \Omega'(k^*)(|k|-k^*) + \frac{\Omega''(k^*)}{2}(|k|-k^*)^2\right], \tag{1}$$

where the right-going wave is picked, $\Omega(|k|) = \sqrt{|k|(1+|k|^4)}$, and the prime denotes the derivative with respect to $|k|$. At the minimum of the phase velocity, it is not difficult to show that the group velocity and phase velocity are equal, namely $\Omega'(k^*) = \Omega(k^*)/k^*$. Therefore, Eq. (1) can be recast to

$$\omega(k) \approx \frac{1}{2}\mathrm{sgn}(k)\left\{\Omega''(k^*)(k^*)^2 + 2\left[\Omega'(k^*) - \Omega''(k^*)k^*\right]|k| + \Omega''(k^*)k^2\right\}, \tag{2}$$

where, specifically,

$$\Omega(k^*) = 2\times 3^{-\frac{5}{8}}, \qquad \Omega'(k^*) = 2\times 3^{-\frac{3}{8}}, \qquad \Omega''(k^*) = 3^{\frac{7}{8}}.$$

By substituting $\mathrm{i}\partial_t$ for ω, $-\mathrm{i}\partial_x$ for k, and $\mathrm{i}\mathcal{H}$ for $\mathrm{sgn}(k)$ in Eq. (2), one obtains a linear dispersive equation

$$\eta_t - 3^{-\frac{3}{8}}\eta_x - \frac{3^{\frac{3}{8}}}{2}\mathcal{H}\left[\eta - 3^{\frac{1}{2}}\eta_{xx}\right] = 0, \tag{3}$$

where η is the surface elevation and $\mathcal{H}$ is the Hilbert transform. We introduce quadratic, cubic, and quartic nonlinearities to complete the equation, yielding

$$\eta_t - 3^{-\frac{3}{8}}\eta_x - \frac{3^{\frac{3}{8}}}{2}\mathcal{H}\left[\eta - 3^{\frac{1}{2}}\eta_{xx}\right] + \alpha\eta\eta_x + \beta\eta^2\eta_x + \gamma\eta^3\eta_x = 0\,, \tag{4}$$

where α, β, and γ are constants. To determine the coefficients of the nonlinear terms, we follow the idea of Akers and Milewski in 2009. First of all, we should match the nonlinear coefficient of the associated cubic NLS equation of Eq. (4) with that of the full Euler equations. It is noted that the quartic term has no contribution in deriving the cubic NLS equation but comes into play while deriving the cubic-quintic NLS equation. Introducing the amplitude parameter ϵ and slowly varying variables $X = \epsilon x$, $T = \epsilon t$, and $\tau = \epsilon^2 t$, we expand the free surface as

$$\eta = \epsilon A(X - c_g T, \tau)\mathrm{e}^{\mathrm{i}(kx-\omega t)} + \epsilon^2 A_2(X - c_g T, \tau)\mathrm{e}^{2\mathrm{i}(kx-\omega t)} + \mathrm{c.c.} + \cdots\,, \tag{5}$$

where $c_g = \frac{1+5k^4}{2\omega}$ is the group velocity and 'c.c.' stands for complex conjugation. We then substitute the ansatz Eq. (5) into Eq. (4) and equate like powers of ϵ. The resulting equation of $O(\epsilon)$ recovers the linear dispersion relation Eq. (2), and the equation associated with $\epsilon^2\mathrm{e}^{2\mathrm{i}(kx-\omega t)}$ gives $A_2 = 3^{-\frac{3}{8}}\alpha k A^2/(\frac{1}{2} - \sqrt{3}k^2)$. On the other hand, if we derive the NLS equation based on the full Euler equations, the expression of A_2 reads $A_2 = \omega^2 A^2/(1 - 14k^4)$. Making these two expressions equal at $k = k^*$ yields $\alpha = \frac{2}{11}\cdot 3^{\frac{3}{8}}$. Finally, the solvability condition for $O\left(\epsilon^3\right)$ results in the cubic NLS equation for A as

$$\mathrm{i}A_\tau + \frac{3^{\frac{7}{8}}}{2}A_{XX} + \left(2\cdot 3^{-\frac{7}{8}}\alpha^2 - 3^{-\frac{1}{4}}\beta\right)|A|^2 A = 0\,. \tag{6}$$

Since the coefficient of the cubic nonlinearity in the associated NLS equation derived from the full Euler equation is $-\frac{79}{88}3^{-\frac{9}{8}}$ (see Refs. [11,12] for example), we then let

$$2\times 3^{-\frac{7}{8}}\alpha^2 - 3^{-\frac{1}{4}}\beta = -\frac{79}{88}3^{-\frac{9}{8}}\,,$$

which gives

$$\beta = 2\times 3^{-\frac{5}{8}}\alpha^2 + \frac{79}{88}3^{-\frac{7}{8}} = \frac{1061}{2904}\times 3^{\frac{1}{8}}\,. \tag{7}$$

It is apparent that if we only include the quadratic nonlinear term $\eta\eta_x$ as done in Ref. [2], then the defocusing NLS equation cannot be expected.

It is challenging to derive the cubic-quintic NLS equation from the full Euler equations. We do not attempt to derive the higher-order NLS equation from the primitive equations or the Whitham type model. Instead, we fix the parameter γ numerically by matching the amplitude of the solitary wave at the bifurcation point (i.e., the pentagram in Fig. 1). It turns out that $\gamma \approx 0.6534$ for this specific problem.

We compute progressive solutions to Eq. (4) based on the standard pseudo-spectral method and the Newton iteration. Assume $\eta(x,t) = \eta(x - ct)$, where c is the translating speed, and hence the governing equation takes the form

$$-\left(c + 3^{-\frac{3}{8}}\right)\eta_\xi - \frac{3^{\frac{3}{8}}}{2}\mathcal{H}\left[\eta - 3^{\frac{1}{2}}\eta_{\xi\xi}\right] + \alpha\eta\eta_\xi + \beta\eta^2\eta_\xi + \gamma\eta^3\eta_\xi = p_\xi\,, \tag{8}$$

where $\xi = x - ct$ and $p(\xi)$ is an external forcing mimicking the constant moving load on the ice sheet. Equation (8) is solved numerically by approximating η with its truncated Fourier series

$$\eta(\xi) = \sum_{n=-N}^{N} a_n\,\mathrm{e}^{\mathrm{i}2\pi n\xi/L}, \tag{9}$$

where the unknown coefficients a_n satisfying $a_n = a_{-n}$ are real for symmetric solutions, and L is the length of the computational domain discretized by $2N+1$ equally distributed grid points. By substituting Eq. (9) into Eq. (8) and projecting the resultant equation onto each element of the basis $\mathrm{e}^{\mathrm{i}2\pi n\xi/L}$ for $n = 0, 1, 2, \cdots, N$, one obtains $N+1$ nonlinear algebraic equations, where the Hilbert transform and derivatives are computed by using the Fourier multipliers. The translating speed c is either prescribed or considered an unknown and solved by adding an extra equation to the discretized system (usually by specifying the wave amplitude which is defined as $(\max\eta - \min\eta)/2$). The solution is considered to converge when the l^∞−norm of the residual error is less than 10^{-10}. The bifurcation curves are computed by straightforward numerical continuation in a chosen parameter (usually the speed, unless a turning point is reached).

We start with computing free bright solitary waves ($p(\xi) = 0$) below the phase speed minimum, whose amplitudes are greater than a specific positive value. In contrast to the results presented in Ref. [11], where only depression solitary waves are found to exist in potential flows coupled with the Kirchhoff-Love elastic model, two types of solitary waves are found in Eq. (8). They are depression solitary waves with a negative central displacement (Fig. 2b) and elevation solitary waves with a positive central displacement (Fig. 3b). We follow the branches of bright solitary waves by increasing the translating speed. As c passes through the bifurcation point $c_{\min}$, the finite-amplitude bright solitary pulse inevitably resonates with a periodic wave of similar speed, resulting in a generalized solitary wave (dashed red lines in Figs. 2a and 3a). These solutions are characterized by a solitary pulse in the middle and trains of ripples on both sides (see Fig. 2c for the depression generalized solitary wave and Fig. 3c for the elevation one). Further numerical experiments show that the algorithm converges well if we add more and more oscillations to the obtained profile. It is shown in Figs. 2c and 3c that the profiles obtained for $L = 62\pi\times 3^{\frac{1}{4}}$ (solid blue lines) are almost exactly on top of the profiles for $L = 82\pi\times 3^{\frac{1}{4}}$ (dotted red lines), which provides strong evidence that these solutions are true generalized solitary waves as the domain size approaches infinity. When the speed further increases, the tails gradually grow and catch up with the solitary pulse in amplitude. And finally, the generalized solitary waves merge in a branch of periodic waves.

As the system is forced by a load moving with constant speed, the solution may reach a steady state in the moving frame when the forcing speed is in a suitable range. To compute these steady solutions, we use the pressure distribution $p(\xi) = \varepsilon\,\mathrm{e}^{-\xi^2/9}$, where ε is a parameter that controls the peak amplitude of the applied pressure, and the results are qualitatively similar for other fully localized distributions. Two representative cases are shown in Fig. 2 for $\varepsilon = 0.02$ (solid blue line) and $\varepsilon = 0.1$ (solid green line). The results agree well with the full Euler computations shown in Ref. [11]. The existence of the moving pressure breaks the symmetry of the bifurcation, with the upper branch being the small perturbation of bright/generalized solitary waves and the lower branch being the small perturbation of the free stream. For large forcing ($\varepsilon = 0.1$), there is a gap between the branch of steady solutions and the bifurcation point, which is termed the 'transcritical regime'. This range of gap will lead to interesting time-dependent dynamics. When the large pressure distribution moves with speed in this range, there is neither a steady forced solution nor a linear mechanism to radiate energy away. Therefore the energy accumulates within the forced region and releases once in the form of solitary waves as the amplitude reaches a certain level. Besides the periodic shedding of solitary waves due to large forcing, another striking phenomenon is the non-existence of transcritical regime for small forcing, indicating that no large responses can be gen-

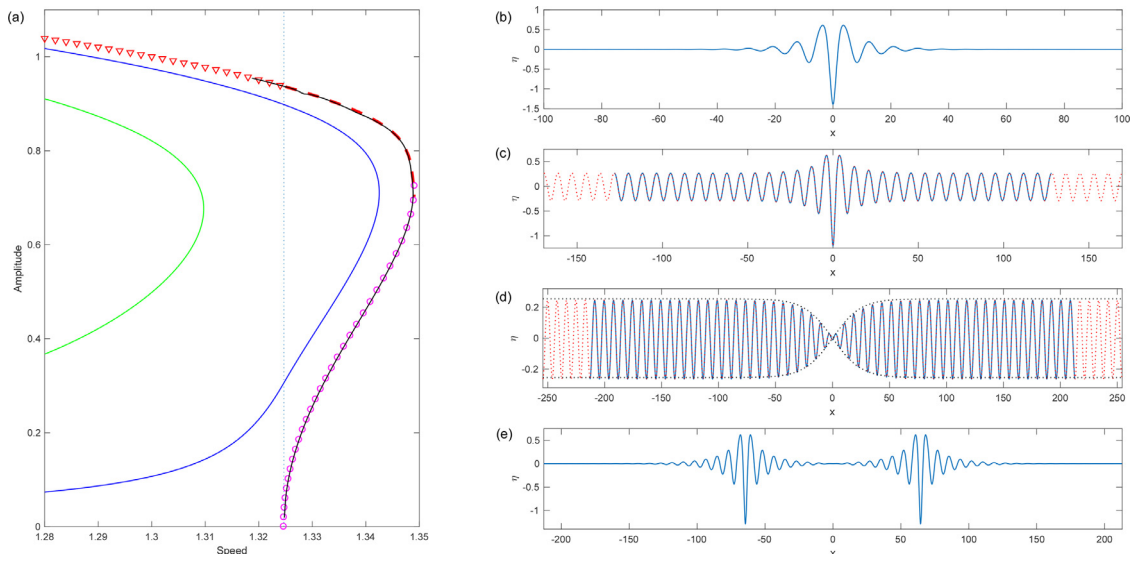

Fig. 2. (**a**) Speed-amplitude bifurcation diagram of depression waves near the phase speed minimum $c_{\min} = 1.3247$ (vertical dotted line). The amplitude is defined as $(\max\eta - \min\eta)/2$. The forced solutions are shown by solid blue and green lines, respectively, for large and small pressure distributions. The free solution branches originating at $c_{\min}$ are periodic Stokes waves (magenta circles) and dark solitary waves (solid black line). The generalized solitary waves (dashed red line) and bright depression solitary waves (downward pointing triangles) appear along the branch of periodic waves. (**b**) A typical profile for bright solitary wave ($c = 1.3$). (**c**) Typical profiles for generalized solitary wave ($c = 1.331$) computed in the domains with lengths $62 \times 3^{\frac{1}{4}}\pi$ (solid blue line) and $82 \times 3^{\frac{1}{4}}\pi$ (dotted red line). (**d**) Typical profiles for dark solitary wave ($c = 1.33$) computed in the domains with lengths $103 \times 3^{\frac{1}{4}}\pi$ (solid blue line) and $123 \times 3^{\frac{1}{4}}\pi$ (dotted red line), respectively; the envelope (dotted black lines) are the NLS prediction. (**e**) A typical profile of multi-packet solitary wave ($c = 1.3187$) arising along the branch of dark solitary waves.

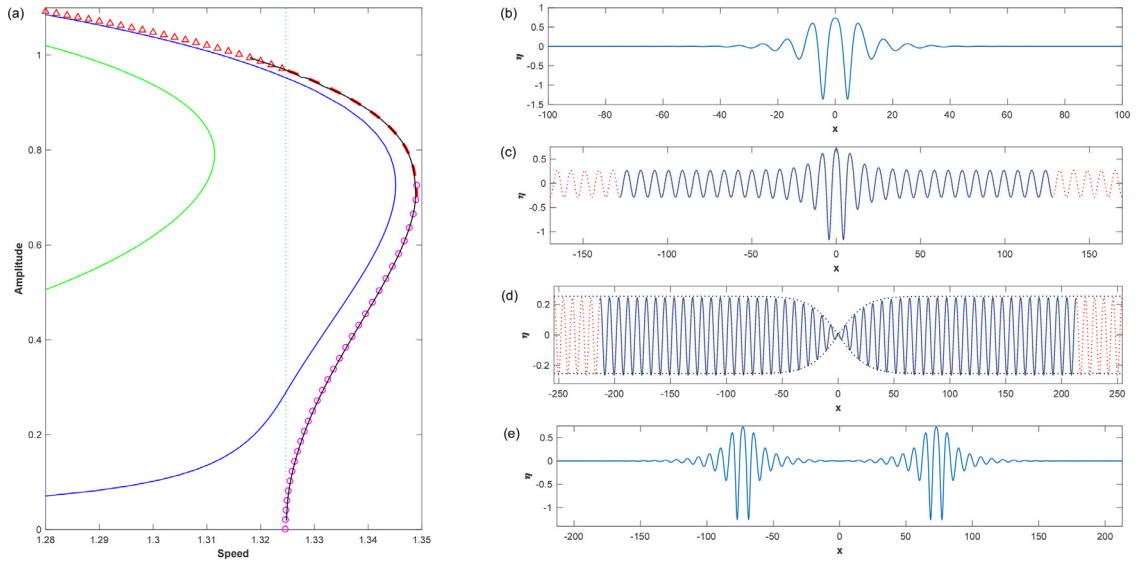

Fig. 3. (**a**) Speed-amplitude bifurcation diagram of elevation waves near the phase speed minimum $c_{\min} = 1.3247$ (vertical dotted line). The amplitude is defined as $(\max\eta - \min\eta)/2$. The forced solutions are shown by solid blue and green lines, respectively, for large and small pressure distributions. The free solution branches originating at $c_{\min}$ are periodic Stokes waves (magenta circles) and dark solitary waves (solid black line). The generalized solitary waves (dashed red line) and bright elevation solitary waves (upward pointing triangles) appear along the branch of periodic waves. (**b**) A typical profile for bright solitary wave ($c = 1.3$). (**c**) Typical profiles for generalized solitary wave ($c = 1.331$) computed in the domains with lengths $62 \times 3^{\frac{1}{4}}\pi$ (solid blue line) and $82 \times 3^{\frac{1}{4}}\pi$ (dotted red line). (**d**) Typical profiles for dark solitary wave ($c = 1.33$) computed in the domains with lengths $103 \times 3^{\frac{1}{4}}\pi$ (solid blue line) and $123 \times 3^{\frac{1}{4}}\pi$ (dotted red line), respectively; the envelope (dotted black lines) are the NLS prediction. (**e**) A typical profile of multi-packet solitary wave ($c = 1.318$) arising along the branch of dark solitary waves.

erated as relatively low-mass vehicles moving close to $c_{\min}$. This is very different from the case of pure gravity waves forced by a moving ship, where the transcritical regime exists regardless of the amplitude of the applied pressure. As shown in Fig. 3a, similar results can be obtained for forced elevation waves (i.e., $\varepsilon = -0.2$ for large forcing and $\varepsilon = -0.02$ for small forcing), which were not observed in Ref. [11].

We now turn to the branch of free dark solitary waves. The defocusing nature of the cubic NLS equation for the present problem predicts the existence of dark solitary waves bifurcating from infinitesimal periodic waves. The dark soliton solution for Eq. (6) takes the form

$$A(X,\tau) = \sqrt{\frac{88}{79}3^{\frac{9}{8}}\Omega}\,\tanh\left(X\sqrt{3^{-\frac{7}{8}}\Omega}\right)\mathrm{e}^{-\mathrm{i}\Omega\tau}\,, \tag{10}$$

where Ω is an arbitrary positive constant. For the free-surface profile, to leading order, one obtains

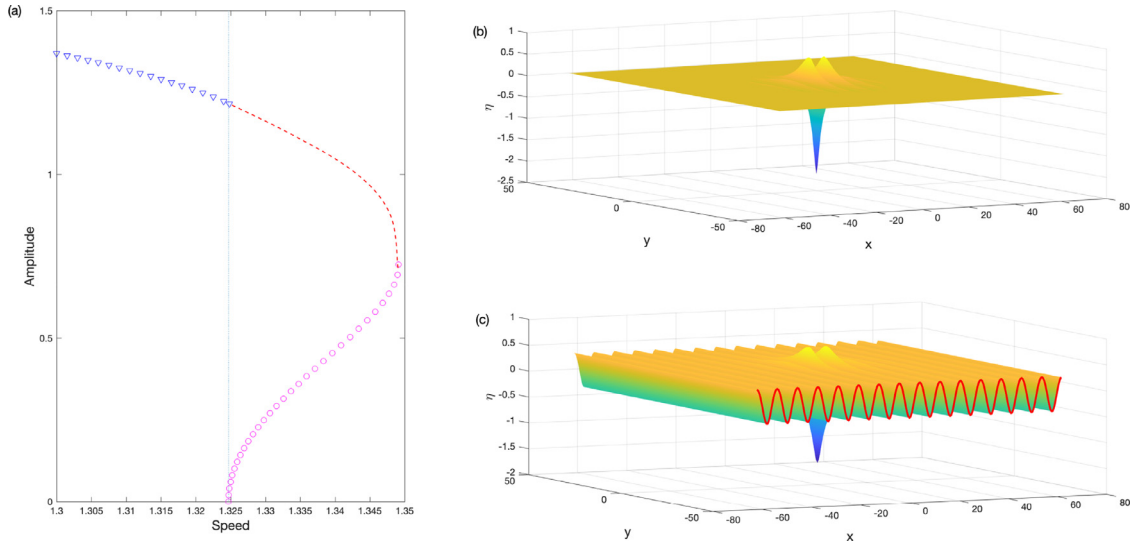

Fig. 4. (**a**) Speed-amplitude bifurcation diagram for free depression lumps (downward pointing triangles), generalized lumps (dashed red line), and periodic waves (pink circles). (**b**) Typical profile of depression lump at $c = 1.3$. (**c**) Typical profile of generalized depression lump at $c = 1.3336$.

$$\eta(x,t) \approx \pm 2\epsilon \sqrt{\frac{88}{79} 3^{\frac{9}{8}} \Omega}\, \tanh\left[\epsilon(x - c_{\min} t)\sqrt{3^{-\frac{7}{8}}\Omega}\right] \times \sin\left[k^*\left(x - c_{\min} t - \frac{\Omega}{k^*}\epsilon^2 t\right)\right], \tag{11}$$

recalling that $k^* = 3^{-\frac{1}{4}}$ and $c_{\min} = 2 \times 3^{-\frac{3}{8}}$. To search for dark solitary waves in Eq. (8), as suggested by Ref. [12], we usually choose $L = (2n+1)\pi/k^*$ to avoid the Newton-Raphson iteration converging to the Stokes wave, where n is a positive integer. For small-amplitude solutions, two types of dark solitary waves are found according to the phase at the center: concave-up (Fig. 2d) and concave down (Fig. 3d). The NLS prediction (11) (dotted black lines in Figs. 2d and 3d) provides excellent approximations for envelopes. The solutions computed with $n = 51$ (solid blue lines) are almost exactly on top of the solutions with $n = 61$ (dotted red lines), indicating that more and more Stokes waves can be added to the tails, hence strongly suggesting the existence of true dark solitary waves. Following the bifurcation curve of dark solitary waves by increasing the wave amplitude, a turning point appears (see solid black lines in Figs. 2a and 3a), through which the solution transits from dark solitary waves to multi-hump generalized solitary waves. After crossing over the bifurcation point from supercritical to subcritical, the solution ultimately becomes multi-packet bright solitary waves, which are characterized by two depression/elevation wavepackets placed side by side (see typical profiles in Figs. 2e and 3e). Although the distance between the packets in the reduced model is larger than that in the Euler equations, these multi-packet solutions are qualitatively similar to the full Euler solution shown at the top of Fig. 1.

It is also possible to generalize Eq. (4) to the three-dimensional hydroelastic wave problem. Let the x-axis be the wave propagation direction, and the y-axis be the horizontal transverse direction. Following Ref. [2], we expand the linear dispersion relation about $(\pm k^*, 0)$ and continue to use the existing nonlinear terms by assuming unidirectional wave propagation with slight inhomogeneity in the transverse direction. One eventually obtains

$$\eta_t - 3^{-\frac{3}{8}}\eta_x - \frac{3^{\frac{3}{8}}}{2}\mathcal{H}\left[\eta - 3^{\frac{1}{2}}\eta_{xx} - 2\cdot 3^{-\frac{1}{2}}\eta_{yy}\right] + \alpha\eta\eta_x + \beta\eta^2\eta_x + \gamma\eta^3\eta_x = 0. \tag{12}$$

The underlying '2+1' NLS equation for Eq. (12) is of defocusing type, which rules out small-amplitude lumps (i.e., spatially confined traveling waves in three dimensions) in Eq. (12). However, as shown in Ref. [16] for interfacial capillary-gravity waves, lump solutions can still exist in a fully nonlinear model in this situation but bifurcate from a non-zero amplitude. In the subsequent computations, we seek lump solutions with symmetry in both x- and y-directions in Eq. (12) based on the standard pseudo-spectral method similar to Eq. (9) (the details of the numerical scheme are omitted, and the interested readers are referred to Refs. [2,16] for reference). The bifurcation diagrams and typical profiles of lumps are shown in Figs. 4a, 4b, 5a and 5b. As indicated by the defocusing NLS equation, no small-amplitude lumps can be found below the minimum of the phase speed. The key observation is that both elevation and depression lumps, which feature oscillatory decaying tails in the propagation direction but monotonic decaying tails in the transverse direction, are found to exist at finite amplitude. However, as the translating speed increases and reaches the supercritical regime, the resonance mechanism results in generalized lumps akin to a lump embedded in a periodic plane wave (see Figs. 4c and 5c). The branches of generalized lumps ultimately join in the branch of Stokes waves; see the bifurcation curves in Fig. 4a for depression waves and Fig. 5a for elevation waves, similar to their two-dimensional counterparts.

In the present paper, we have proposed a phenomenological model for describing the bifurcation mechanism of deep-water hydroelastic waves by generalizing the Whitham equation. The fundamental idea is to fix the coefficients of the quadratic and cubic terms by matching the cubic NLS equation derived from the model with that from the full Euler equations and determine the coefficient of the quartic nonlinearity by matching the amplitude of the solitary wave at the bifurcation point. The newly proposed model can capture the primary features of the bifurcation mechanism in the vicinity of the phase speed minimum. This approach can easily be generalized to include the effects due to inertia, vorticity, and viscoelasticity for the problem of moving loads on ice sheets. More generally, this idea can be extended to other nonlinear wave problems in fluid dynamics, such as interfacial gravity-capillary waves, surface waves with constant vorticity, electrocapillary-gravity waves, etc.

Finally, we should point out that much remains to be improved for the Whitham type models. Particularly, the selection of non-

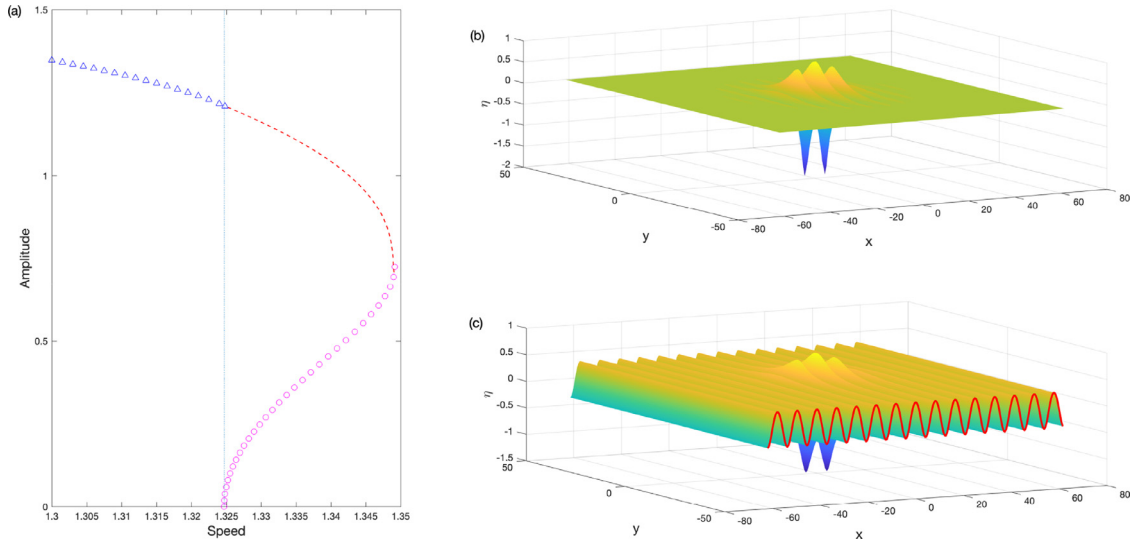

Fig. 5. (**a**) Speed-amplitude bifurcation diagram for free elevation lumps (upward pointing triangles), generalized lumps (dashed red line), and periodic waves (pink circles). (**b**) Typical profile of elevation lump at $c = 1.3$. (**c**) Typical profile of generalized elevation lump at $c = 1.3336$.

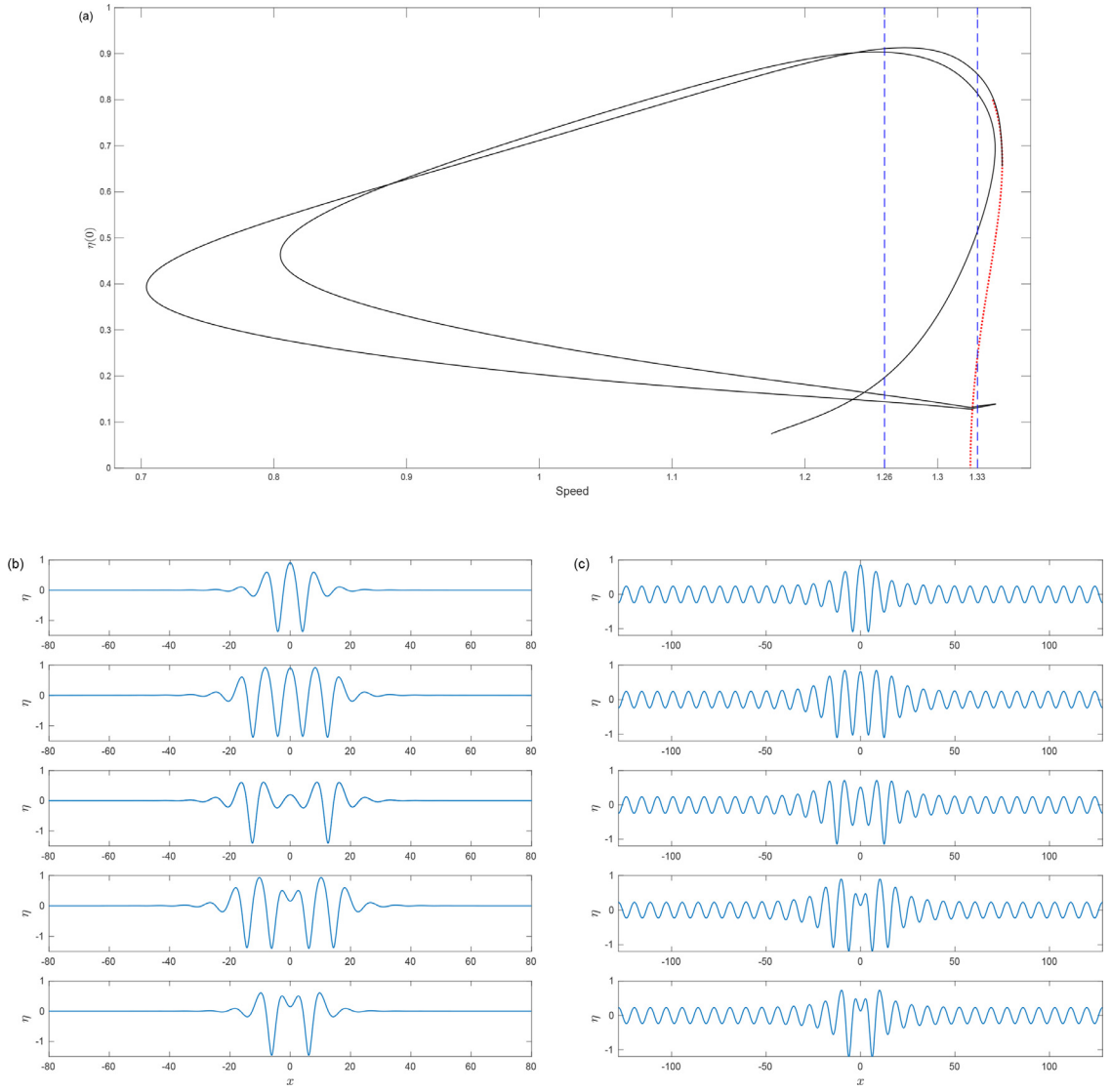

Fig. 6. (**a**) Solution diagrams for free elevation waves (solid dark line) and periodic waves (dotted red line) in the quadratic-cubic-quintic model. The free-surface amplitude $\eta(0)$ is plotted against wave speed. (**b**) Bright solitary waves at $c = 1.26$ corresponding to the intersection points from top to bottom between the left-hand vertical dashed line and the elevation branch shown in (**a**). (**c**) Generalized solitary waves at $c = 1.33$ corresponding to the intersection points from top to bottom between the right-hand vertical dashed line and the elevation branch shown in (**a**).

linear terms is artificial in Eq. (4) to some extent, though the approach adopted in the paper has certain rationality and feasibility. For example, we can choose quadratic, cubic, and quintic nonlinear terms and fix the coefficients based on the method mentioned. It is not difficult to obtain

$$\eta_t - 3^{-\frac{3}{8}}\eta_x - \frac{3^{\frac{3}{8}}}{2}\mathcal{H}\left[\eta - 3^{\frac{1}{2}}\eta_{xx}\right] + \alpha\eta\eta_x + \beta\eta^2\eta_x + \widetilde{\gamma}\eta^4\eta_x = 0\,, \tag{13}$$

where α and β are the same as Eq. (4), and $\widetilde{\gamma} \approx -0.6935$. This model can capture most features near the bifurcation point; however, in contrast to the full Euler equations, the branch of dark solitary waves in this model does not lead to multi-packet bright solitary waves. Nevertheless, the quadratic-cubic-quintic model shows good agreement with the Euler equations in some other aspects away from the bifurcation point. For example, the elevation branch in Eq. (13) exhibits the characteristic 'snake-like behavior' shown in Fig. 6a: the speed-amplitude bifurcation curves show a zigzag behavior with multiple turning points. The most striking phenomenon is that the bifurcation curve is trans-regional. As it reaches the supercritical regime, non-decaying wavetrains appear on wave profiles; see the comparison between bright solitary waves (Fig. 6b) and generalized solitary waves (Fig. 6c). This phenomenon was also observed for hydroelastic waves with constant vorticity [7]. Overall, it is of great interest to find a systematic/rigorous method to choose nonlinear terms for the Whitham type equations, which we leave for future investigations.

Declaration of Competing Interest

We declare that we have no financial and personal relationships with other people or organizations that can inappropriately influence our work, there is no professional or other personal interest of any nature or kind in any product, service and/or company that could be construed as influencing the position presented in, or the review of, the manuscript submitted.

Acknowledgments

This work was supported by the National Natural Science Foundation of China under Grant No.11772341 and the Strategic Priority Research Program of the Chinese Academy of Sciences under Grant No. XDB22040203.

References

[1] D.S. Agafontsev, F. Dias, E.A. Kuznetsov, Deep-water internal solitary waves near critical density ratio, Physica D 225 (2007) 153–168.
[2] B. Akers, P.A. Milewski, A model equation for wavepacket solitary waves arising from capillary-gravity flows, Stud. Appl. Math. 122 (2009) 249–274.
[3] T.R. Akylas, Envelope solitons with stationary crests, Phys. Fluids A 5 (1993) 789–791.
[4] T.B. Benjamin, A new kind of solitary wave, J. Fluid Mech. 245 (1992) 401–411.
[5] Y. Cho, J.D. Diorio, T.R. Akylas, J. Fluid, et al., Resonantly forced gravity-capillary lumps on deep water. part 2. theoretical model, Mech. 672 (2011) 288–306.
[6] F. Dias, G. looss, Capillary-gravity interfacial waves in infinite depth, Eur. J. Mech. B/Fluids 15 (1996) 367–393.
[7] T. Gao, P.A. Milewski, J.M. Vanden-Broeck, Hydroelastic solitary waves with constant vorticity, Wave Motion 85 (2019) 84–97.
[8] O. Laget, F. Dias, Numerical computation of capillary-gravity interfacial solitary waves, J. Fluid Mech. 349 (1997) 221–251.
[9] Z. Lin, Y. Zhu, Z. Wang, Local bifurcation of electrohydrodynamic waves on a conducting fluid, Phys. Fluids 29 (2017) 032107.
[10] N. Masnadi, J.H. Duncan, The generation of gravity-capillary solitary waves by a pressure source moving at a trans-critical speed, J. Fluid Mech. 810 (2017) 448–474.
[11] P.A. Milewski, J.-M. Vanden-Broeck, Z. Wang, J. Fluid, Hydroelastic solitary waves in deep water, Mech. 679 (2011) 628–640.
[12] P.A. Milewski, J.-M. Vanden-Broeck, Z. Wang, Steady dark solitary flexural gravity waves, Proc. R. Soc. A 469 (2013) 20120485.
[13] V. Squire, R.J. Hosking, A.D. Kerr, et al., Moving Loads on Ice Plates, Solid Mechanics and Its Applications, Kluwer (1996).
[14] V. Squire, W. Robinson, P. Langhorne, et al., Vehicles and aircraft on floating ice, Nature 333 (1988) 159–161.
[15] E.I. Părău, F. Dias, Nonlinear effects in the response of a floating ice plate to a moving load, J. Fluid Mech. 460 (2002) 281–305.
[16] Z. Wang, H. Meng, M. Vanden-Broeck, A quasi-planar model for gravity-capillary interfacial waves in deep water, Stud. Appl. Math. 133 (2014) 232–256.
[17] G.B. Whitham, Linear and Nonlinear Waves, John Wiley & Sons, 1974.